Asymmetric Transport Efficiencies of Positive and Negative Ion Defects in Amorphous Ice

Eui-seong Moon, Youngsoon Kim, Sunghwan Shin, and Heon Kang*

Department of Chemistry, Seoul National University, 1 Gwanak-ro, Seoul 151-747, Republic of Korea

(Received 3 February 2012; published 29 May 2012)

Hydronium (H_3O^+) ions at an ice surface penetrate into its interior over a substantially longer distance than hydroxide (OH^-) ions. The observation was made by conducting reactive ion scattering and infrared spectroscopic measurements for the acid-base reaction between surface H_3O^+ (or OH^-) and NH_3 (or NH_4^+) trapped inside an amorphous ice film at low temperature (< 100 K). The study reveals very different transport efficiencies of positive and negative ion defects in ice. This difference is explained by the occurrence of an efficient proton-relay channel for H_3O^+, which does not exist for OH^-.

DOI: 10.1103/PhysRevLett.108.226103 PACS numbers: 68.49.Sf, 42.68.Ge, 66.30.jp, 72.20.Jv

Ice is a unique type of solid conductor containing hydronium (H_3O^+) and hydroxide (OH^-) ions as intrinsic charge carriers. These species exist as positive and negative ion defects, respectively, in the ice lattice where they are in proton-transfer equilibrium with constituting water molecules. It is generally conceived that the coexistence of positive and negative ionic defects is deeply related to certain unusual electrical properties of ice, including the thermoelectric effect [1] and the freezing potential (the Workman-Reynolds effect) [2,3]. The properties of ion defects in ice are an appealing subject of study not only from the perspective of ice physics, but also in a broad range of disciplines in physics, environmental sciences, astrophysics, and chemistry owing to the ubiquity and importance of ice in natural environments.

Numerous studies have been performed to understand the charge conduction phenomena of ice [4–13]. The experimental studies range from classical ice conductivity measurements [4] to modern molecular spectroscopic measurements that monitor the H/D isotopic exchange kinetics and proton-transfer dynamics [5–11]. The theory of charge conduction in terms of ice molecular structure was advanced by Jaccard [12] and Onsager and Dupuis [13] long ago. Owing to these investigations, the transport mechanism of H_3O^+ in ice is now well understood. H_3O^+ moves via a sequence of proton transfers along the hydrogen bond chain of water (Grotthuss mechanism), and this process may occur even at low temperature. At high temperature, the proton-transfer relay is coupled with Bjerrum defect motion to extend the distance of the proton transfers [5–7]. However, a complete picture for charge conduction in ice will be attainable only when the transports of both positive and negative ion defects are properly understood. The present study explores some open questions related to this issue: What is the relative efficiency of charge transport by positive and negative ion defects? Do they move like ''mirror images'' in ice with only the proton-transfer directions reversed, or via intrinsically different molecular mechanisms? To answer these questions, we have measured the transport distances of H_3O^+ and OH^- through an ice film by placing H_3O^+ (or OH^-) at the ice film surface and its counter base (or acid) in the ice interior. The study shows that H_3O^+ travels a substantially longer distance than OH^- due to the occurrence of an efficient proton-relay mechanism for H_3O^+, which does not exist for OH^-.

We conducted the experiment in an ultrahigh vacuum chamber [14] equipped with instrumentation for reactive ion scattering (RIS), low-energy sputtering (LES), reflection absorption infrared spectroscopy (RAIRS), and temperature programmed desorption (TPD). An H_2O ice film was grown typically to a thickness of 50 BL (bilayer; 1 BL $= 1.14 \times 10^{15}$ water molecules cm^{-2}) on a Ru(0001) crystal by using a back-filling method at a slow (≤ 0.1 BL s^{-1}) deposition rate. The Ru substrate temperature was maintained at 70–100 K, which resulted in an amorphous ice film growth [15]. The thickness of the ice film was estimated by performing TPD measurements [16]. HCl and NH_3 vapors were introduced into the chamber through separate leak valves and guided close to the sample surface through tube dosers. Cs atoms were deposited onto the sample by using an alkali metal dispenser (SAES Getters).

The chemical species present on the ice film surface were measured by performing RIS, LES, and RAIRS analyses. In the RIS and LES experiments, a Cs^+ beam from a low-energy ion gun (Kimball Physics) collided with the sample surface at the incident energy of 30 eV, and the ions emitted from the surface were detected by a quadrupole mass spectrometer (Extrel) with its ionizer filament switched off. In RIS, *neutral* species (X) on the surface are picked up by the scattering of Cs^+ projectiles to form Cs^+-neutral clusters (CsX^+). In LES, preformed *ionic* species (Y^+ and Z^-) on the surface are ejected by the Cs^+ impact. Thus, RIS and LES signals reveal the identities of neutral (X) and ionic species (Y^+ and Z^-), respectively, on the surface [14,17]. The probing depth for LES and RIS methods is $\sim$1 BL of the ice surface at the employed Cs^+ beam energy [17]. Chemical species in the interior of the ice samples were monitored with RAIRS [18,19].

We studied the transport of H_3O^+ by preparing an ice film that had excess hydronium ions on its surface and proton acceptor (NH_3) molecules in the interior at a controlled distance from the surface (sample *A*). Figure 1 shows the results of LES, RIS, and RAIRS measurements performed at each preparation stage of sample *A*. First, an amorphous H_2O-ice film (50 BL thickness) was grown on Ru(0001), and NH_3 was adsorbed onto the film surface for a coverage of ~0.3 ML. The presence of NH_3 and H_2O molecules on the surface was verified by the RIS signals of $CsNH_3^+$ ($m/z = 150$) and CsH_2O^+ ($m/z = 151$), shown in Fig. 1(I-a), and the ν_2 band (umbrella mode; 1100 cm^{-1}) of NH_3 [20] in the RAIR spectrum, shown in Fig. 1(II-a). Next, an H_2O layer was overlaid on the sample for a desired thickness between 3–30 BL to make an NH_3-sandwich ice film. In Fig. 1(b), where the H_2O overlayer thickness was thin (3 BL), the $CsNH_3^+$ signal intensity decreased to a certain degree, indicating that NH_3 molecules were partially buried under the H_2O layer. The ν_2 band intensity of NH_3 corresponding to the total NH_3 content in the sample did not decrease. The added H_2O layer increased the IR band intensity around 1600 cm^{-1}, which corresponded to the intramolecular bending mode of H_2O.

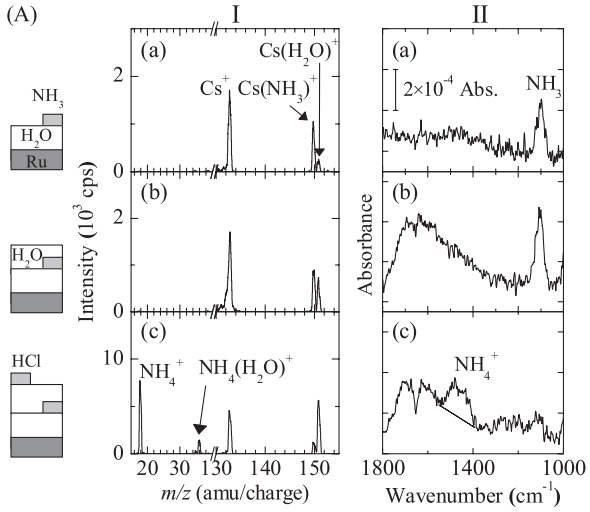

FIG. 1. (I) Mass spectra of LES and RIS signals obtained at each preparation stage of sample *A* ($H_3O^+/H_2O/NH_3/H_2O$ film). (II) The corresponding RAIR spectra. The sample was prepared in the following sequence. (a) An H_2O-ice film (50 BL thickness) was grown on Ru(0001), and NH_3 was adsorbed on the surface for a coverage of ~0.3 ML. (b) An H_2O film (3 BL) was overlaid onto the surface. (c) HCl was adsorbed for ~0.2 ML at 90 K to generate H_3O^+ on the surface. The Ru substrate temperature was kept at 90 K or below during the construction of the sample. The RAIR spectra correspond to the "difference spectra" with respect to a pure H_2O film (50 BL). The spectral absorbance is indicated by the scale bar in spectrum (II-a). The dotted line in spectrum (II-c) is drawn as a guide to the eye.

Finally, HCl was added onto the $H_2O/NH_3/H_2O$ film, which produced H_3O^+ and Cl^- on the surface via HCl ionization [17]. This created a situation in which H_3O^+ was located at the sample surface and the proton acceptor (NH_3) was buried underneath the H_2O overlayer. The H_2O overlayer thickness defined the distance between the proton donor and acceptor. Thermal diffusion of NH_3 in the ice film was observed to be negligible at temperature $\leq$ 90 K, which is consistent with the diffusion coefficient of NH_3 in ice reported in the literature [21,22]. H_3O^+ has a thermodynamic tendency to reside at the ice surface rather than in the interior [7,11]. The IR spectrum obtained from this sample [Fig. 1(II-c)] showed a new band appearing near 1470 cm^{-1}, which corresponded to the ν_4 band of NH_4^+ [23]. The NH_3 signal intensity at 1100 cm^{-1} decreased. These changes revealed that NH_3 was converted to NH_4^+ by the proton transfer from surface H_3O^+ species (reaction 1).

$$H_3O^+(s) + NH_3(b) \rightarrow H_2O(s) + NH_4^+(b), \quad \text{(reaction 1)}$$

where (*s*) and (*b*) indicate surface and bulk species, respectively. The LES spectrum [Fig. 1(I-c)] showed an NH_4^+ peak ($m/z = 18$), which indicated that NH_4^+ was formed on the film surface as well as in the interior. The amount of the surface NH_4^+ species (measured by LES) was estimated to be 55% of the total NH_4^+ content (measured by RAIRS) for this sample. Importantly, the H_3O^+ signal ($m/z = 19$) was absent from the LES spectrum, which revealed that the proton transfer from H_3O^+ to NH_3 was complete.

The transport phenomena of OH^- were studied by conducting analogous experiments to those described above for H_3O^+ transport. The difference was that the ice sample used for the OH^- study contained excess OH^- species on its surface and counter acid (NH_4^+) in the sandwich layer (sample *B*). This sample was prepared as follows. On the surface of an H_2O-ice film (50 BL) grown on Ru(0001), NH_3 (0.30 ML) and HCl (0.25 ML) were coadsorbed to produce NH_4^+ via HCl ionization and the subsequent acid-base reaction of H_3O^+ and NH_3. The NH_4^+ signal in the LES spectrum [Fig. 2(I-a)] and the 1470 cm^{-1} band of NH_4^+ in the IR spectrum [Fig. 2(II-a)] confirmed the formation of NH_4^+. A small excess of NH_3 remained unreacted on the surface, which was indicated by the $CsNH_3^+$ peak in Fig. 2(I-a) and the NH_3 signal (1100 cm^{-1}) in Fig. 2(II-a), although H_3O^+ was all consumed in the acid-base reaction, as evidenced by the absent H_3O^+ signal. Next, an H_2O overlayer was deposited for a desired thickness between 3–30 BL to make an NH_4^+-sandwich film. Figure 2(b) illustrates the results for an H_2O overlayer with 3–4 BL thickness. The NH_4^+ signal disappeared from the LES spectrum, whereas the IR signal of NH_4^+ did not decrease but rather somewhat sharpened. These changes indicated that the H_2O overlayer

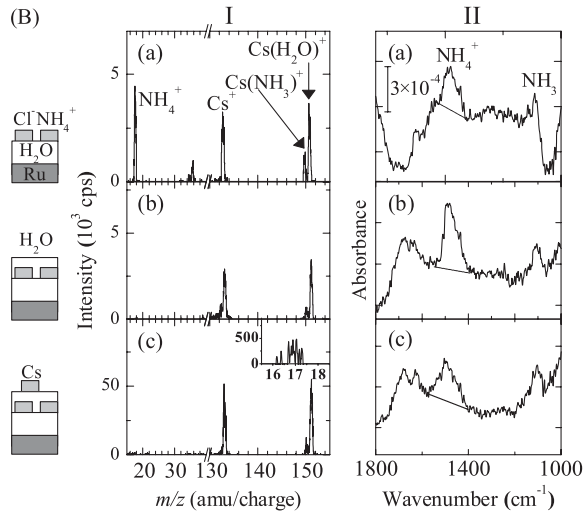

FIG. 2. (I) LES and RIS mass spectra obtained at each preparation stage of sample B ($OH^-/H_2O/NH_4^+/H_2O$ film). (II) The corresponding RAIR spectra. (a) NH_3 (0.30 ML) and HCl (0.25 ML) were coadsorbed on an amorphous H_2O-ice film (50 BL thickness) to generate NH_4^+. (b) An H_2O overlayer (3–4 BL) was added to make an NH_4^+-sandwich ice film. (c) OH^- species (0.15 ML) were provided by the hydrolysis of Cs atoms on the surface. The temperature was maintained at ~80 K during the sample construction. The dotted lines in the RAIR spectra are provided as a guide to the eye.

completely covered the NH_4^+. The NH_4^+ band sharpening was due to the additional solvation of NH_4^+ by H_2O [24].

Excess OH^- was added onto the surface of the NH_4^+-sandwiched film by adsorbing Cs atoms. The Cs adsorbates hydrolyzed to Cs^+ and OH^- ions on the ice surface. Both Cs^+ and OH^- stay on the surface of a pure ice film [25,26]. The RAIR spectrum from this sample [Fig. 2(II-c)] showed that the NH_4^+ intensity at 1470 cm^{-1} somewhat decreased upon the addition of OH^- on the surface. This indicated the occurrence of the reaction between OH^- and NH_4^+. However, the NH_3 intensity at 1100 cm^{-1} did not increase, indicating that the reaction occurred without the formation of NH_3. Therefore, we consider that the reaction led to salt formation via the direct association of NH_4^+ and OH^- (reaction 2).

$$OH^-(s) + NH_4^+(b) \rightarrow NH_4OH(b) \qquad \text{(reaction 2)}$$

The unchanging NH_3 intensity indicates that the proton transfer from interior NH_4^+ to surface OH^- did not occur. Further, this indicates nonoccurrence of the OH^- transport via a proton-transfer relay across the H_2O film. The migration of OH^- is required by (reaction 2). In this case we consider that OH^- can move via molecular hydroxide diffusion, as observed in a recent study of OH^- transport in amorphous ice at ~135 K [26]. The diffusion of NH_4^+ is prohibited in the sample [Fig. 2(b)]. In the negative-ion LES spectrum [inset of Fig. 2 (I-c)], an OH^- signal appeared with a low intensity, indicating that (reaction 2) did not occur to completion.

The transport distances of H_3O^+ and OH^- in ice were measured by repeating the experiments described above with ice samples that had various thicknesses of an H_2O spacer, i.e., by changing the separation distance between H_3O^+ (or OH^-) and NH_3 (or NH_4^+). Experimentally, we measure the yield of the acid-base reaction as a function of the distance of the acid-base pair, and this reaction yield is equivalent to the transport efficiency (η) of H_3O^+ or OH^- across the distance because the reaction goes to completion upon the contact of the acid-base pair. The transport efficiency was calculated according to Eqs. (1a) and (1b).

$$\eta(H_3O^+) = \frac{\Delta\theta_s(H_3O^+)}{\theta_s^{\text{initial}}(H_3O^+)} = \frac{\Delta\theta_b(NH_3)}{\theta_s^{\text{initial}}(HCl)} \qquad \text{(1a)}$$

$$\eta(OH^-) = \frac{\Delta\theta_s(OH^-)}{\theta_s^{\text{initial}}(OH^-)} = \frac{\Delta\theta_b(NH_4^+)}{\theta_s^{\text{initial}}(Cs)} \qquad \text{(1b)}$$

Here, $\eta(X)$ is the transport efficiency of X, and θ_s and θ_b are surface and bulk populations, respectively. For example, $\eta(H_3O^+)$ is equivalent to the change of relative surface population of H_3O^+, which, in turn, is estimated from the decrease of NH_3 population in the interior measured by RAIRS. Figure 3 displays $\eta(H_3O^+)$ and $\eta(OH^-)$ measured as functions of the H_2O spacer thickness. The result indicates that H_3O^+ transports over a substantially longer distance than OH^-.

The experimentally measured transport distance needs to be refined by making a correction for the nonuniform thickness of the H_2O spacer film. The H_2O film has microscopic variations in its thickness mainly for two reasons: (i) deposition of randomly incident water molecules and (ii) difference in sticking probability of water on H_2O, NH_3, and NH_4^+ adsorbates. The thickness variation due to the first factor can be simulated by using a stochastic model for film growth from randomly incident gas molecules (Supplemental Material 1 [27]). The thickness

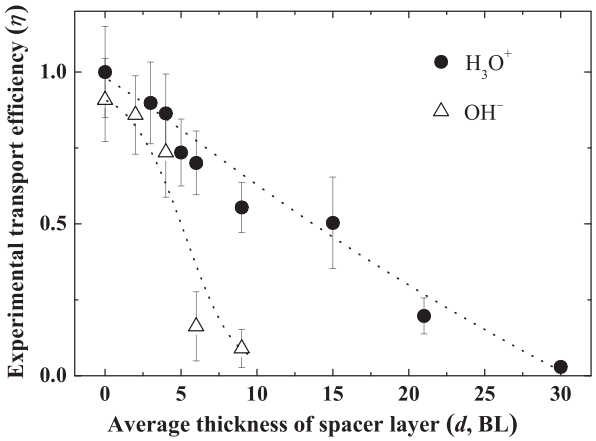

FIG. 3. Experimental measurement for the transport efficiencies of H_3O^+ (•) and OH^- (△) as a function of H_2O spacer thicknesses (d). The temperature was ~80 K during the experiment. The dotted lines are provided as a guide to the eye.

distribution function thus obtained is shown in Eq. (2), where $P(l;d)$ represents the probability that the film has a local thickness of l when its average thickness is d.

$$P(l;d) = \left(\frac{d^l}{l!}\right)\exp(-d) \tag{2}$$

Equation (2) was validated by comparing it with the experimental growth behavior of a D_2O overlayer on an H_2O film. Second, the sticking probability of water on various adsorbate sites was estimated by performing separate adsorption experiments. The sticking probability was ~1.0 on H_2O and NH_4^+, and ~0.14 on NH_3. This means that, for sample A, the H_2O overlayer grew thinner on NH_3 than on H_2O, and some NH_3 adsorbates could remain exposed to the surface, as observed in Fig. 1(b). In this case, the proton-transfer distance from H_3O^+ to NH_3 was shorter than the average thickness of the spacer layer. Also, NH_4^+ could be formed on the surface as well as in the interior. The correction procedure accounting for this effect is described in Supplemental Material 2 [27]. For sample (B), this correction was unnecessary because the water sticking probability was the same on both the H_2O and NH_4^+ sites. With these considerations, the relationship between the experimentally measured transport efficiency (η) and a corrected transport efficiency (η') is given by Eq. (3).

$$\eta(d) = \sum_l P_{\text{spacer}}(l;d)\eta'(l) \tag{3}$$

Here, $P_{\text{spacer}}(l;d)$ is the thickness distribution function of a spacer film after making the correction for surface NH_4^+ species. A corrected transport efficiency (η') curve was obtained by fitting a theoretical $\eta(d)$ function in Eq. (3) to the experimental $\eta(d)$ curve. A least-mean-square method was used for the fitting so as to minimize the difference between the experimental and theoretical $\eta(d)$ curves, $\sum[\eta_{\text{exp}}(d) - \eta_{\text{theory}}(d)]^2$, from which an optimized set of $\eta'(l)$ values were deduced.

Figure 4 displays the corrected transport efficiency (η') of H_3O^+ and OH^- as a function of the actual transport distance (l). η' is close to unity at short distances ($\leq$ 3 BL) for both H_3O^+ and OH^-. In contrast to the rapid drop of $\eta'(OH^-)$ to zero at $l \sim 6$ BL, $\eta'(H_3O^+)$ remains substantially high (~ 0.4) until it tails off at ~24 BL. The substantially longer travel distance of H_3O^+ than OH^- clearly indicates their asymmetric transport behaviors. It is well known [12,13] that H_3O^+ moves via a proton hopping relay from H_3O^+ to the neighboring water molecules along the hydrogen bond chain, and that the associated energy barrier is very small [28]. For OH^- transport, however, an analogous "mirror image" mechanism of proton relay does not operate, according to the present observation that proton transfer does not occur between the separated NH_4^+ and OH^- species. The nonoccurrence of a proton-relay mechanism for OH^- transport may be attributed to the rigid structure of ice [29], in contrast to the facile occurrence of this mechanism in liquid water due to solvent fluctuation [30].

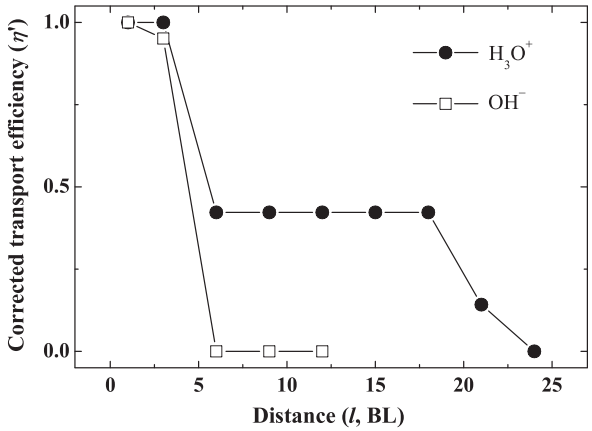

FIG. 4. The corrected transport efficiency (η') of H_3O^+ (•) and OH^- (□) as a function of the separation distance (l) of acid and base.

It is worthwhile mentioning a few additional aspects of the present study. First, the measurements were made with amorphous ice samples, where abundant defect sites act as proton traps and thus block the transport path of H_3O^+. For this reason, the transport distance of H_3O^+ is expected to be significantly longer in crystalline ice than in amorphous ice. OH^- transport distance would not increase in an ice crystal but may in fact decrease because molecular diffusion is more difficult. Therefore, the difference between the H_3O^+ and OH^- transport distances is expected to be amplified for ice crystals. The low temperature requirement for the present experiment does not allow us to prepare a crystalline ice sample and check this behavior. Second, H_3O^+ [7,11] and OH^- [25,26] reside preferentially at the surface of ice in equilibrium states due to their thermodynamic affinities for the surface. Dynamically, however, these species may commute from the ice surface to its interior depending on their mobility. This work measures such travel distances by monitoring the trapping events of H_3O^+ (or OH^-) at NH_3 (or NH_4^+) sites in the ice interior.

Third, H_3O^+ and OH^- were produced on the ice film surfaces by the hydrolysis of HCl and Cs, respectively, which are exoergic. The energy released from these reactions may induce local heating of the surface and promote the transport of ions over a short range before the energy is dissipated into the lattice. It is possible that the near unity values of $\eta'(H_3O^+)$ and $\eta'(OH^-)$ appearing at $l \leq 3$ BL are due to this effect. Because the energy release is greater for the formation of OH^- (75 kJ mol^{-1}) than H_3O^+ (61 kJ mol^{-1}), its promotion effect may be greater for OH^- than for H_3O^+. However, our observation for $l > 3$ BL is the opposite, which means that the extra energy effect does not interfere with the key conclusion that H_3O^+ has a longer transport distance than OH^-.

In summary, the measurement for the travel ranges of H_3O^+ and OH^- in amorphous ice at low temperature demonstrates their asymmetric transport efficiencies. H_3O^+ migrates across a much longer distance than OH^- due to an efficient proton relay involving H_3O^+. On the other hand, an analogous proton-relay channel does not operate for OH^-. Instead, molecular hydroxide diffusion can occur to a limited extent. Such behaviors are drastically different from their mirror image picture. The observation has several implications. H_3O^+ is a uniquely mobile species in low temperature ice, where molecular diffusion is effectively frozen and OH^- can have only a limited migration distance. As such, the acid-base reactions involving H_3O^+ may be important for the chemistry of ice in terrestrial and space environments at low temperature [23,31], whereas the activity of OH^- is less important except for its role as a proton-transfer inhibitor [29]. In addition, the asymmetric mobility of H_3O^+ and OH^- may be able to provide a better understanding for the charge imbalance phenomena of ice, including its thermoelectric effect [2,3] and the charging of ice surfaces [1]. Also, the present observation made for amorphous ice in the absence of solvent fluctuation may offer an interesting checkpoint for the study of H_3O^+ and OH^- transport dynamics in liquid water [30,32].

This work was supported by the National Research Foundation grant funded by the government of Korea (MEST) (2007-0056333).

*Corresponding author.
surfion@snu.ac.kr

[1] P. V. Hobbs, *Ice Physics* (Clarendon Press, Oxford, 1974), Chaps. 2 and 9.
[2] E. J. Workman and S. E. Reynolds, Phys. Rev. **78**, 254 (1950).
[3] T. Takahash, J. Atmos. Sci. **26**, 1253 (1969).
[4] V. F. Petrenko and R. W. Whitworth, *Physics of Ice* (Oxford University Press, Oxford; New York, 1999), Chaps. 4 and 5.
[5] W. B. Collier, G. Ritzhaupt, and J. P. Devlin, J. Phys. Chem. **88**, 363 (1984).
[6] P. J. Wooldridge and J. P. Devlin, J. Chem. Phys. **88**, 3086 (1988).
[7] C. W. Lee, P.-R. Lee, Y.-K. Kim, and H. Kang, J. Chem. Phys. **127**, 084701 (2007).
[8] A. Uritski, I. Presiado, Y. Erez, R. Gepshtein, and D. Huppert, J. Phys. Chem. C **113**, 10 285 (2009).
[9] J. Blomquist, M. P. Andersson, and P. Uvdal, Phys. Rev. Lett. **107**, 216101 (2011).
[10] I. Presiado, J. Lal, E. Mamontov, A. I. Kolesnikov, and D. Huppert, J. Phys. Chem. C **115**, 10 245 (2011).
[11] Y. Lilach, M. J. Iedema, and J. P. Cowin, Phys. Rev. Lett. **98**, 016105 (2007).
[12] C. Jaccard, Helv. Phys. Acta **32**, 89 (1959).
[13] L. Onsager and M. Dupuis, *The Electrical Properties of Ice in Electrolytes*, edited by B. Pesce (Pergamon Press, Oxford, 1962), pp. 27–49.
[14] H. Kang, Bull. Korean Chem. Soc. **32**, 389 (2011).
[15] A. Hodgson and S. Haq, Surf. Sci. Rep. **64**, 381 (2009).
[16] D. N. Denzler, S. Wagner, M. Wolf, and G. Ertl, Surf. Sci. **532**, 113 (2003).
[17] H. Kang, Acc. Chem. Res. **38**, 893 (2005).
[18] Y. J. Chabal, Surf. Sci. Rep. **8**, 211 (1988).
[19] M. Trenary, Annu. Rev. Phys. Chem. **51**, 381 (2000).
[20] A. Kouchi and T. Kuroda, Nature (London) **344**, 134 (1990).
[21] N. Uras and J. P. Devlin, J. Phys. Chem. A **104**, 5770 (2000).
[22] F. E. Livingston, J. A. Smith, and S. M. George, J. Phys. Chem. A **106**, 6309 (2002).
[23] W. A. Schutte and R. K. Khanna, Astron. Astrophys. **398**, 1049 (2003).
[24] C. J. Pursell, M. Zaidi, A. Thompson, C. Fraser-Gaston, and E. Vela, J. Phys. Chem. A **104**, 552 (2000).
[25] J. H. Kim, Y. K. Kim, and H. Kang, J. Phys. Chem. C **113**, 321 (2009).
[26] S. Kim, E. Park, and H. Kang, J. Chem. Phys. **135**, 074703 (2011).
[27] See Supplemental Material at http://link.aps.org/supplemental/10.1103/PhysRevLett.108.226103 for details of the thickness distribution model (1) and the estimation of the sticking probability (2).
[28] C. Kobayashi, S. J. Saito, and I. Ohmine, J. Chem. Phys. **113**, 9090 (2000).
[29] L. Cwiklik, J. P. Devlin, and V. Buch, J. Phys. Chem. A **113**, 7482 (2009).
[30] D. Marx, A. Chandra, and M. E. Tuckerman, Chem. Rev. **110**, 2174 (2010).
[31] E. S. Moon, H. Kang, Y. Oba, N. Watanabe, and A. Kouchi, Astrophys. J. **713**, 906 (2010).
[32] K. J. Tielrooij, R. L. A. Timmer, H. J. Bakker, and M. Bonn, Phys. Rev. Lett. **102**, 198303 (2009)